HYDRODYNAMIC SIMULATION OF THE SUEZ CANAL; A WATER BODY CONNECTING TWO OPEN SEAS

M.A. ELZEIR[1], and T.HIBINO[2]

[1]Visiting researcher, Port and Harbour Research Institute, 3-1-1 Nagase, Yokosuka, 239-0826 Japan; Dr. Eng. Lecturer, Civil Engineering Department, El-Minia University, El-Minia, Egypt.
[2]member of JSCE, Dr.Eng. Senior research engineer, Marine Environment Division, PHRI, 3-1-1 Nagase, Yokosuka,239-0826 Japan.

The Suez Canal is an important water-transport route all over the world. Two hydrodynamic issues related to the flow within the canal are worthy of consideration: sedimentation in the northern section of the canal and high velocity current in the southern section of the canal. To address the sedimentation issue, a large program of dredging works is being undertaken. A numerical model is presently being developed to simulate flow in the canal with a special attention paid to the south part. This model is the focus of the present study. The model is a two-dimensional depth averaged finite element model utilizing independent open boundaries at the north and south ends of the canal. The radiation and modified long wave boundary conditions are compared. Due to its accuracy and flexibility to suit different forcing conditions, the radiation boundary condition shows superiority over the modified long-wave formulation. The simulation results reflect most of the physical phenomena observed in the canal.

Keywords: *Hydrodynamic, Suez Canal, radiation, MOLWAF, open boundary condition, finite element.*

1. INTRODUCTION

The Suez Canal is a vital waterway connecting the Far East and Europe, allowing ships to pass from the Mediterranean to the Indian Ocean and vise versa without having to navigate around the Cape of Good Hope. It is an artificial waterway running north to south across the Isthmus of Suez in northeastern Egypt. It connects the Mediterranean Sea with the Gulf of Suez, an arm of the Red Sea (**Fig. 1**). The average ship transit time in the canal is about 15 hours, with average speed of 13 to 14 km/hr. In the southern sector the speeds vary between 11 and 15 km/hr depending on the velocity and direction of the tidal current. The canal consists of three components; the north canal, the Bitter Lakes and the south canal.

The canal is approximately 163 km long. It is the longest unlocked channel in the world, as the Mediterranean Sea and the Gulf of Suez have roughly the same water level and the Suez Isthmus is a part of the flat desert of the Sinai Peninsula. Excavation of the canal began in 1859 and the canal was opened to navigation in 1869. The Mediterranean Sea at the north of the canal is an enclosed sea of Europe, Asia, and Africa, linked to the Atlantic Ocean at its western end by the narrow strait of Gibraltar. The Mediterranean is almost land locked and is generally shallow. An undersea sill at the strait of Gibraltar restricts circulation between the sea and the ocean. Moreover, evaporation is not compensated for by fresh water inflows. Therefore, the sea is much saltier than the Atlantic Ocean. Mediterranean waters are warm and tides tend to be weak. The Red Sea is, also, a narrow enclosed sea separating the Arabian Peninsula, in western Asia, from northeastern Africa. It extends north west from the strait of Bab el-Mandeb to Suez (south entrance of the Suez Canal) for a distance of about 2253 km. The northern extremity is divided into the Gulfs of Suez and Aqaba by the Sinai Peninsula (**Fig. 1 a**).

Navigation in the canal is very safe because the canal is straight, deep and has no locks,. Hydrodynamic issues will be addressed in section two. A combination of numerical modeling and field observations was used to analyze these difficulties. Sections 3 to 5 discuss the modeling techniques. The third section of the paper explains a 2D depth-averaged finite element model. The fourth section discusses the open boundary conditions and applies the radiation Open Boundary Condition (OBC) to the finite element model. In the fifth section, the model is applied to the Suez Canal with two different forcings at the open boundaries. The last section will conclude the paper.

2. HYDRODYNAMICS OF SUEZ CANAL

The hydrodynamics of the canal has two main distinct features. Firstly, at the north entrance,

sediment carried by the Mediterranean waters is deposited in the canal. Therefore, the canal is permanently dredged to maintain a reasonable water depth for navigation. The ongoing dredging program is highly successful in preventing siltation from affecting navigation. Secondly, the current in the south reach of the canal (extending between the Bitter Lakes and the Gulf of Suez (**Fig.1 b**)) attains periodically fast speed. At present, the means by which these fast currents are generated is poorly understood. It is this second problem that is the focus of this research.

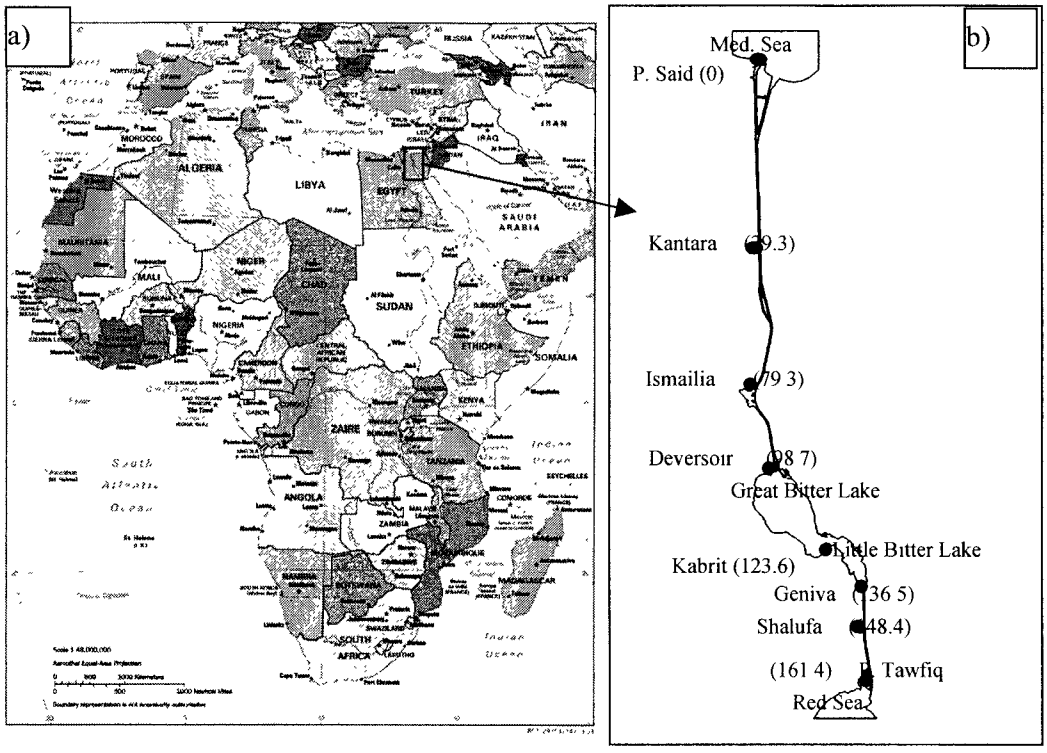

Fig. 1: Suez Canal: a) Geographic location b) schematic. Number in brackets is distance in km from Port Said.

3. GOVERNING EQUATIONS AND DISCRETIZATION SCHEME

The governing equations of shallow water flow are

$$\frac{\partial U_i}{\partial t} + U_j U_{i,j} + g\,\zeta_{,i} + \frac{\tau_i^b}{\rho(h+\zeta)} - A_l (U_{i,j} + U_{j,i})_{,j} + f_i = 0 \qquad (3\text{-}1a)$$

$$\frac{\partial \zeta}{\partial t} + [(h+\zeta)\, U_j]_{,j} = 0 \qquad (3\text{-}1b)$$

where **U** is the mean horizontal velocity, ζ is the water elevation, h is the mean water depth, g is the gravitational acceleration, A_l is the eddy viscosity and **f** is the Coriolis force. The bottom friction can be given as

$$\tau_i^b = \frac{n^2 g}{h^{1/3}} U_i (U_k U_k)^{1/2} \qquad (3\text{-}2)$$

where n is the Manning coefficient.

In the above and following equations, standard index-notation is used and the usual summation convention with repeated indices is employed. The assumptions underlying the above mentioned equations are as follows. The Navier-Stokes equations are integrated over the depth assuming hydrostatic pressure distribution. The Reynolds stresses together with the viscosity term are modeled by a constant eddy viscosity term.

The finite element model developed by Kashiyama et al.[1] is used in the current study. The three node linear triangular element is used for spatial discretization. The bottom friction term is linearized. For discretization in time, the three-step explicit time integration scheme is used. The selective lumping parameter is used as follows.

$$M_{\alpha\beta}^S = e\, M_{\alpha\beta}^L + (1\text{-}e)\, M_{\alpha\beta} \qquad (3\text{-}3)$$

where $M_{\alpha\beta}$ is the consistent mass matrix, $M_{\alpha\beta}^L$ is the lumped mass matrix, $M_{\alpha\beta}^S$ is the selectively lumped mass matrix, and e is a selective lumping parameter, between zero and one. Selective lumping combines the advantages of the consistent formulation, which does not damp the numerical solution but produces spatial oscillations, with that of the lumped formulation, which produces no oscillations through the introduction of excessive diffusive effects, and therefore may smear the results.

4. BOUNDARY CONDITIONS

Numerical models of finite domains (as part of the infinite real world domain) inevitably involve the treatment of boundaries where the numerical grid ends. Boundaries generally fall into one of two categories: solid boundaries and open boundaries. Solid boundaries are real physical boundaries. They are generally easily dealt with, except perhaps for

movable boundaries; for example, those used in modeling flooding and drying[2]. On the other hand, open boundaries have an obscure physical interpretation, as the hydrodynamic behavior of the modeled domain is dependent on the hydrodynamics outside the domain; however, the numerical behavior of the environment in the region outside the computational domain cannot be known. Thus, some kind of extrapolation of knowledge obtained in the interior of the domain must be used. The specification of the OBC depends on, among others, the character of the equation to be solved; hyperbolic, parabolic or elliptic[3]. For flow problems dominated by advection and/or wave motion, the OBCs should be transparent; that is, they should allow propagating waves which are generated within the computational domain to pass through with minimum reflection and/or distortion. Unfortunately, there is no numerical treatment of open boundaries which achieves this ideal for general models which include two (or three) dimensions, rotation, variable depth, bottom friction, and wind stress forcing[4]. Consequently, it has been suggested that using approximate "ad hoc" OBC may be the most reasonable approach to the problem at this time[5].

Once a reflected wave has been generated, it will remain in the interior domain either until damped out by bottom friction or upon encountering another open boundary where some of the wave energy will be transmitted through the boundary and some will be reflected. Bottom friction alone is not very effective for wave dissipation in space or time and should not be relied upon to remove undesired reflected numerical wave energy. Therefore, we rely on the OBCs to remove numerical oscillations; however, the OBC must, also, be used to input the external forcings representing the interaction of the modeled region with the external environment[2),3)].

Since any ad hoc OBC will introduce inaccuracies into the numerical solution, it is important, for each numerical application, to evaluate a number of OBCs and to choose the most effective one[4].

An OBC that is applied extensively in finite element models[6),7),1)] is stated as:

$$U_n = \zeta^I \frac{g}{\sqrt{gh}} \qquad (4\text{-}1)$$

where U_n is the mean velocity over depth normal to the open boundary, ζ^I is the incident wave height and $\sqrt{gh}$ is the surface gravity wave speed. Condition (4-1) is not sufficient to allow reflected waves to be transmitted through the open boundary because it accounts only for the incident wave while the reflected (numerical) wave is not considered at all. In other words, this condition is a clamping OBC. The following two alternative OBCs have been proposed.

(1) Modified Long Wave Formulation (MOLWAF)

Kodama et al.[8] criticized Eq. (4-1) as it does not allow the outgoing waves to be transmitted through the open boundary. They proposed another OBC[8),9)]. In their OBC, U_n is divided into two parts. U_n^I and U_n^R where I and R represent Incident and Reflected waves respectively. To determine U_n^R, the incident wave height inside the domain must be specified. In the modified long wave formulation, the wave height computed by the model at the open boundaries, ζ^{cal}, comprises two parts; ζ^I and ζ^R, where ζ^I is obtained from known tidal levels and ζ^R is determined as:

$$\zeta^R = \zeta^{cal} - \zeta^I \qquad (4\text{-}2)$$

Consequently, U_n at the open boundary is also divided into two parts:

$$U_n^I = \zeta^I \frac{g}{\sqrt{gh}} \qquad (4\text{-}3)$$

and

$$U_n^R = \begin{cases} 0 & \text{if } \zeta^R \le 0 \\ \zeta^R \dfrac{g}{\sqrt{gh}} & \text{if } \zeta^R > 0 \end{cases} \qquad (4\text{-}4)$$

Equation (4-4) indicates that if a numerical wave is propagating from inside the domain ($\zeta^R>0$), it is allowed to be transmitted through the open boundary; otherwise ($\zeta^R\le0$), no waves are allowed to travel across the open boundary towards inside the domain.

(2) Radiation OBC

for the MODWAF, the water level elevation must be specified at the open boundary, which is not easy. Moreover, the boundary is not perfectly transparent. On the other hand, the Sommerfeld radiation condition[4] is defined as:

$$\phi_{,t} + C\,\phi_{,n} = 0 \qquad (4\text{-}5)$$

where ϕ is the variable to be defined at the open boundary (either U or ζ) and C is the phase speed (or advection velocity). This scheme is more flexible allowing the possibility of different prescriptions for C. The condition was successfully applied in finite difference schemes. However, finite element modelers have been wary of applying this technique for fear of difficulty in its implementation[9]. Unfortunately, use of this technique leads the water level in the model to fall.

One form of the condition, defined by Blumberg and Kanta[10] for a finite difference scheme, is used here with the finite element scheme. In this form, C is taken equal to the local, flat bottom, shallow

water, surface gravity wave speed,

$$C = \sqrt{gh} \qquad (4\text{-}6)$$

Blumberg and Kanta[10] added an ad hoc friction-like term $(\frac{-\phi}{T_f})$ on the right hand side of Eq (4-5) where T_f is a friction time scale. The friction-like term was added as a means of slowing the fall in water level within the domain. The friction time scale T_f is to be estimated by numerical experiment

A boundary element is defined as a finite element that has at least one of its sides coincides with the open boundary. The coordinates of the nodes of the boundary element are transformed from the Cartesian coordinates to the local n-s coordinates (**Fig. 2**).

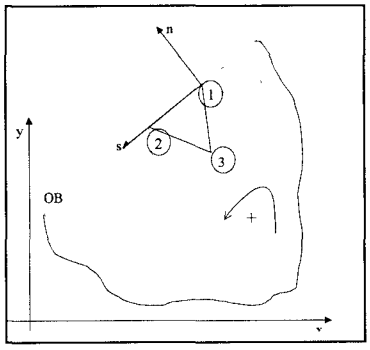

Fig. 2: Axes convention for the radiation OBC

5. SUEZ CANAL FLOW SIMULATION

The mesh developed for the Suez Canal consists of 5169 nodes and 8574 elements. Numerical experiments for a simple channel case showed that the MOLWAF was less accurate than the radiation OBC. Therefore, only the latter was adopted for the Suez Canal case with T_f=5 hours, e=0, A_f=10 m^2/s, n=0.04 and latitude (for Coriolis term)=30.5° N. The data used for model calibration for the present study is water level observations during the year 1997 at four stations within the canal; Port Said, Kantara, Geniva and Shalufa (**Fig. 1**). The data increment is 30 minutes over a 50-hour period. The variation, taking place outside the canal, in the open seas, was not monitored. With the available data, two short-term runs are conducted. The first run was used to develop reasonable boundary forcings using synthetic boundary conditions. The second run was a real world simulation.

Run 1: the forcing tide at both north and south open boundaries was described by:

$$\zeta = A \sin \omega t \qquad (6\text{-}1)$$

where A is the wave amplitude (1.5 m) and ω is the wave frequency $(\frac{2\pi \text{ radians}}{12 \text{ hours}})$. A $\frac{\pi}{2}$ radians lag was adopted from the south to north OBCs. The simulation was carried out for 24 hours.

From **Fig. 3**, it can be seen that, under these conditions, the water in the Bitter Lakes is virtually stagnant. Therefore, the north and south forcings have very little interaction along the canal. It appears that the tide developed at the Red Sea only propagates up to Kabrit while the tide developed at the Mediterranean Sea only propagates down to Deversoir. The velocity in the south reach of the canal (south to the Bitter Lakes) is relatively large when compared with that developed in the north reach under similar forcing conditions. This result is in agreement with the known behavior of the canal as discussed in Section 2.

The wave amplitude at Port Said is 83% of that applied at the Mediterranean open boundary with a lag of 40 minutes. The wave amplitude at Port Tawfiq is 90% of that applied at the Red Sea with a lag of 10 minutes. It should be noted that the distance from the Mediterranean open boundary to Port Said is 8500 m and that from Red Sea open boundary to Port Tawfiq is 10500 m and the depth at the open boundary of the Mediterranean is 20 m approaching the shore with a mild gradient while a depth of 7 m prevails in the Red Sea, apart from the Suez Canal navigation channel, which is considerably deeper. No tide data is available at Port Tawfiq; therefore, lag and decrease in amplitude for Shalufa were also determined. The tide amplitude at Shalufa is 52% of that at the Red Sea with a lag of 38 minutes. Moreover, at Shalufa, the positive tide amplitude is 8 cm larger than the negative one.

Run 2: a simulation was carried out for a period of 49.5 hours starting on 0:00 hours of 9 March, 1997. Since there is no observation data in the open seas, the tide at the open boundary was estimated from the results of run 1. The tidal height at the Red Sea open boundary is taken as 1.92 times that observed at Shalufa and 38 minutes ahead and the tidal height at the Mediterranean Sea open boundary is taken as 1.20 times that observed at Port Said and 40 minutes ahead.

The simulation results at both Port Said and Shalufa coincide well with the observations (**Fig. 4**). However, the results should be taken with caution since the observations at these two stations are used to estimate the open boundary forcing. The observations and simulations at Geniva are in phase (**Fig. 5**); however, the observed tide has positive amplitude of 12 cm and negative one of 35 cm (referred to a common datum for the whole canal). The positive part of the wave exhibits sudden changes, which are not justified physically. The calculated tide, on the other hand, has positive amplitude of 45 cm and negative one of 40 cm. At the middle of the Great Bitter Lake, the positive (calculated) amplitude is 10 cm. The negative observed amplitude at Geniva is in good agreement with that calculated, while the positive observed amplitude is comparable to that calculated at the middle of the Great Bitter Lake. At Kantara, the

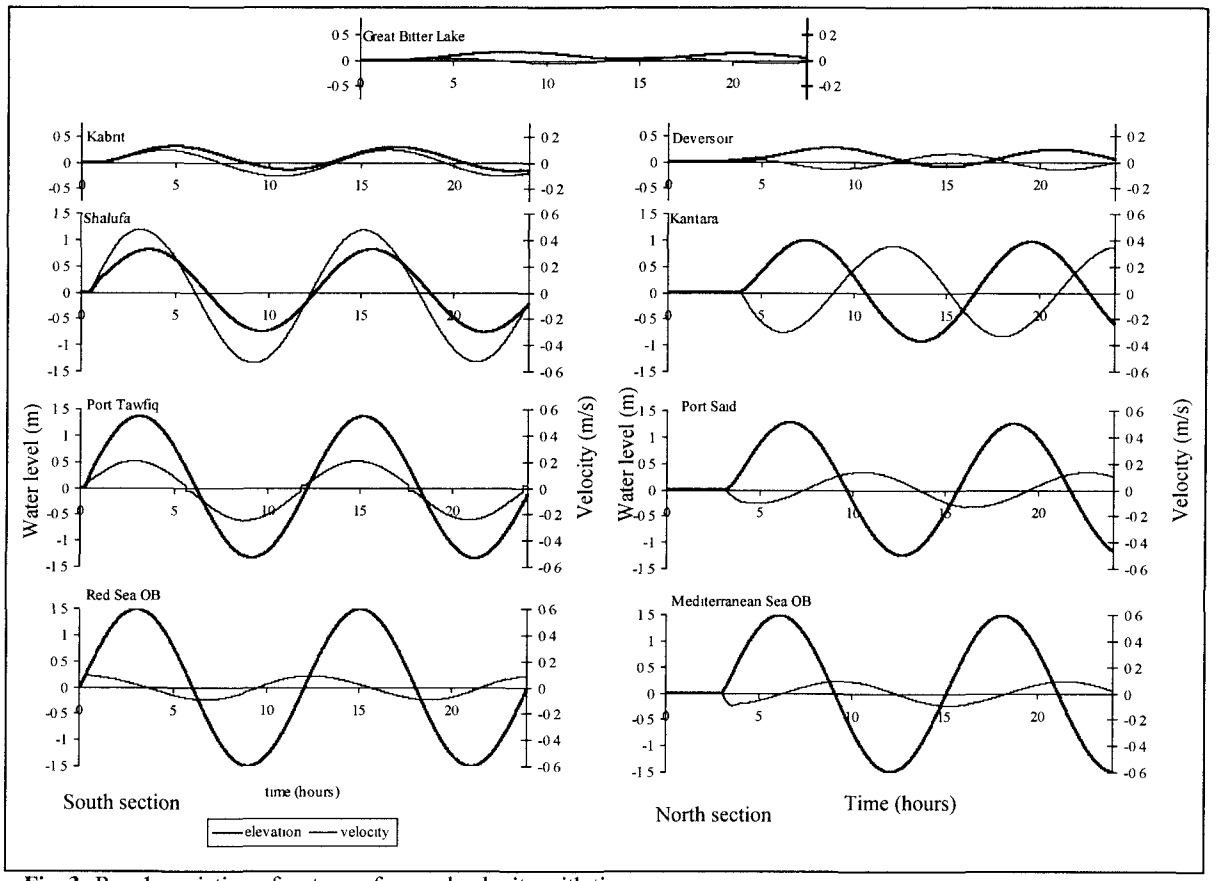

Fig. 3: Run 1: variation of water surface and velocity with time

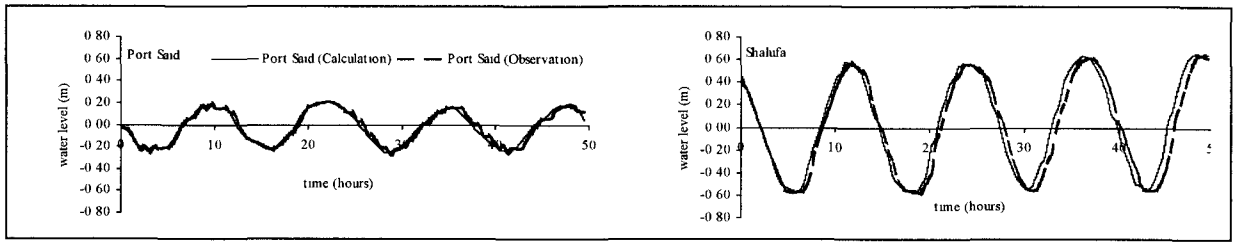

Fig. 4: Run 2: comparison between observation and simulation at Port Said and Shalufa

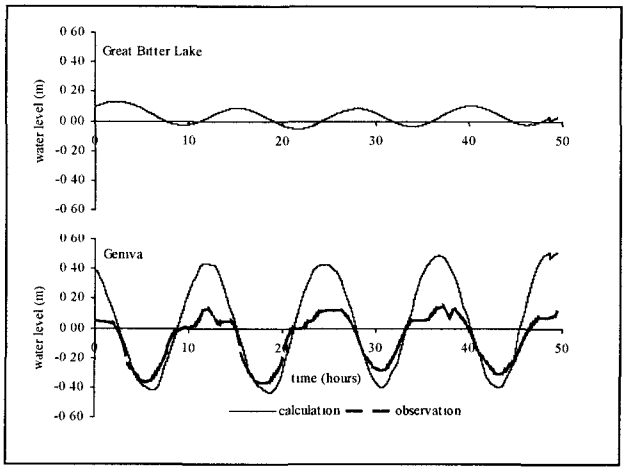

Fig. 5: Run 2: Comparison between Geniva and the Bitter Lake

observations revealed the existence of two consecutive peaks (with the same sign) and strong oscillations although the flow in the canal is (relatively) slowly changing. This phenomena is not observed in any other station. The larger observed peak lags 150 minutes behind the calculated results (**Fig. 6**). The calculated wave at Ismailia (30 km south of Kantara) reasonably matches the observation at Kantara. These differences between model behavior and observations are to be reconciled.

Unfortunately, there are no detailed observations for velocity in the canal. The simulation shows that the maximum velocity takes place in the south reach of the canal (Port Tawfiq to Geniva). The maximum value at Port Tawfiq is 0.16 m/s, at Shalufa is 0.39 m/s and at Geniva is 0.33 m/s. The velocity elsewhere is less than 0.10 m/s. The profiles along the canal (**Fig. 7**) show that the south reach of the canal experiences tides of higher amplitude and faster current than that experienced in the north reach. The maximum velocity is a direct result of the steep slope of the water surface in the south reach of the canal as compared to slopes elsewhere in the canal. These results are all in good agreement with the known behavior of the canal.

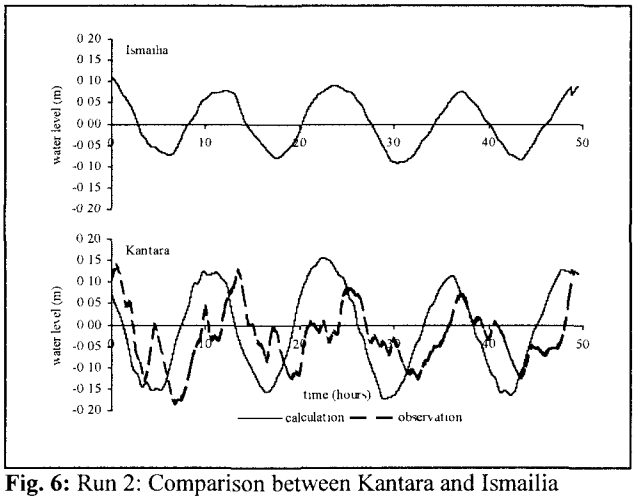

Fig. 6: Run 2: Comparison between Kantara and Ismailia

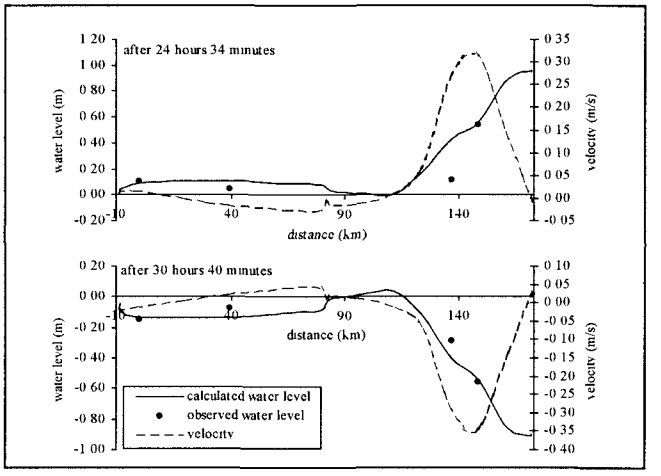

Fig. 7: Run 2: Profiles along the canal. For distance, see Fig. 1

6. CONCLUSION

The Suez Canal is an internationally important artery for water-transport. With the aid of limited observations, it was possible to simulate the canal hydrodynamically using a 2D depth-averaged finite-element model. Two OBCs were trialed, the MOLWAF proving less accurate than the radiation OBC. Moreover, the radiation OBC has the flexibility of tuning the friction time scale as a calibration parameter.

A pilot run for the Suez Canal was used to calibrate the model parameters (e and T_f) and to suggest suitable open boundary forcings. A simulation run was performed based on tuning and boundary forcings from the pilot run. From the simulation, it is clear that the hydrodynamic model with its flexible radiation OBC is capable of predicting the characteristics of the canal flow with reasonable accuracy, in the event that extensive field data is able to be obtained.

ACKNOWLEDGEMENT: The authors are endebted to the group of Dr. Kashiyama, Chuo University, Tokyo, Japan who provided the mesh generator and the basic structure of the finite element model. The data regarding Suez Canal is quoted from the following sites of the internet: Encarta Encyclopedia[11] and CIA Center for African Studies[12]. The leaflets and drafts of observation data obtained from the Suez Canal Authority, Egypt are also acknowledged.

REFERENCES

1) Kashiyama, K., Ito, H., Behr, M. and Tezduyar, T.: Three-Step Explicit Finite Element Computation of Shallow Water Flows on a Massively Parallel Computer, *International Journal for Numerical Methods in Fluids*, Vol.21, pp 885-900, 1995.

2) Lorenzzetti, J. A. and Wang, J. D.: On the Use of Wave-Absorbing Layers in the Treatment of Open Boundaries in Numerical Coastal Circulation Models, *Appl. Math. Modeling*, Vol.10, pp 339-345, 1986.

3) Orlanski, I.: A Simple Boundary Condition for Unbounded Hyperbolic Flows, *J. Computational Physics*, Vol.21, pp 251-269, 1976.

4) Chapman, D. C.: Numerical Treatment of Cross-Shelf Open Boundaries in a Barotropic Coastal Ocean Model, *J. Physical Oceanography*, Vol.15, pp 1060-1075, 1985.

5) Bennett, A. F. and McIntosh: Open Ocean Modeling as an Inverse Problem: Tidal Theory, *J. Phys. Oceangr.*, Vol.12, pp 1004-1018, 1982.

6) Koutitas, C., and O'Conner, B.: Modeling Three-Dimensional Wind-Induced Flows, *J Hydr Div, ASCE*, Vol.106 (HY11), pp 1843-1865, 1980.

7) Kawahara, M., Hirano, H., and Tsubota, K: Selective Lumping Finite Element Method for Shallow Water Flow *International Journal for Numerical Methods in Fluids*, Vol.2, pp 89-112, 1982.

8) Kodama, T., Kawasaki, and Kawahara, M.: Finite Element Method for Shallow Water Equation Including Open Boundary Condition, *International Journal for Numerical Methods in Fluids*, Vol.13, pp 939-953, 1991.

9) Kodama, T., Kawahara, M.: Multiple Level Finite Element Analysis for Tidal Current Flow with Non-Reflective Open Boundary Condition, *JSCE*, No. 446/I-19, pp 77s-87s, 1992.

10) Blumberg, A. F., and Kanta, L. H.: Open Boundary Condition for Circulation Models, *J. Hydr. Eng., ASCE*, Vol.111(2), pp 237-255, 1985.

11) Encarta Online Home:
http://encarta.msn.com/EncartaHome.asp.

12) Index of African Studies, CIA maps:
http://www.sas.upenn.edu/African_Studies/CIA_Maps.

(Received September 30, 1998)